JOURNAL OF MAGNETIC RESONANCE 77, 536–549 (1988)

Noise in High-Power, High-Frequency Double-Tuned Probes

F. D. DOTY, T. J. CONNICK, X. Z. NI, AND M. N. CLINGAN

Doty Scientific, Inc., 600 Clemson Road, Columbia, South Carolina 29223

Received August 3, 1987

Linear, nonlinear, and spurious noise sources are analyzed from the perspective of the design of high-power double-tuned NMR probes. An absolute efficiency is derived for simplified SNR comparison between various probes. A simple, accurate Q measurement technique based on 7 dB return loss is derived. A trilevel proton power decoupling scheme is proposed for reducing certain types of high-voltage noise, and the effects of various joining techniques on high-current shot noise are compared. © 1988 Academic Press, Inc.

INTRODUCTION

The trend toward higher B_0 fields in double-tuned NMR probes for solids has pushed RF engineering to the limit of the technology and has brought to awareness nonlinear effects not anticipated in "linear" circuits. That is, in a circuit consisting only of inductors, capacitors, and resistors, all voltages are linear functions of current. As such, it should be possible to apply very high power at one frequency without introducing noise at the second frequency in a double- or triple-tuned circuit. This may in fact be accomplished up to the point that the circuit remains linear. When the power level being applied at one frequency is hundreds of watts, a very small nonlinearity is sufficient to introduce an unacceptable level of noise at another frequency. The purpose of this paper is to examine some high-voltage and high-current nonlinear mechanisms and to review briefly other noise sources including thermal, triboelectric, and spurious effects. A trilevel proton power scheme is proposed to reduce some sources of high-voltage noise in high-power CP MAS experiments.

THERMAL NOISE

Since Hoult and Richards's now classic treatment (*1*) of S/N in NMR, it has been customary to invoke Lorentz's well known but elusive principal of reciprocity (*2*) to calculate the emf induced in a coil by a magnetic dipole. This principle (often encountered in antenna theory) when applied to NMR transmit–receive coils states that the efficiency of generating RF fields by an arbitrary coil at any point is equivalent to the efficiency of receiving a signal from a precessing dipole located at that point. Precisely stated, the signal S induced in an arbitrary coil by an arbitrary distribution of magnetic dipoles of uniform magnetization M (or susceptibility χ) precessing at an angle ϕ with respect to the static field $B_0\hat{z}$ at angular frequency ω throughout a sample volume V_s may be expressed (*3*) in terms of the circularly polarized transverse field

0022-2364/88 $3.00

component $B_T(\mathbf{r})$ generated throughout that volume by a current I flowing through the coil as follows (mks):

$$S = \frac{\chi B_0 \omega}{\mu_0 I} \int_s \sin \phi B_T(\mathbf{r}) dV. \quad [1]$$

The above equation requires a determination of the circularly polarized transverse component of the magnetic field generated by current I (usually 1/2 of a linearly polarized field) and a knowledge of the magnetization angle ϕ through the volume. The latter is readily determined once the former is known by the following relationship:

$$\phi = \gamma B_T t. \quad [2]$$

The thermal, or Johnson, rms noise voltage N generated by a resistance R in the coil loop is readily derived from first principles (*4*) as

$$N = (4RkT\Delta f)^{1/2}, \quad [3]$$

where Δf is the bandwidth in hertz, R is the resistance at frequency f and temperature T, and k is Boltzman's constant. Hence, the signal-to-noise ratio is

$$S/N = \frac{\chi B_0 \omega V_s}{\mu_0 (4RkT\Delta f)^{1/2}} \frac{\langle B_T \sin \phi \rangle}{I}, \quad [4]$$

where we have assumed that B_T and sin ϕ are reasonably uniform over the sample volume V_s so that the integral may be replaced with an average value $\langle B_T \sin \phi \rangle$.

It is useful to write a simplified expression for the S/N that is valid for comparing different coils or resonators under similar experimental conditions. Assume constant sample characteristics and B_0. Further assume that Δf is established by constant filters much narrower than the bandwidth of the coil or resonator and that B_T is nearly uniform over the sample volume. Then,

$$S/N = k_s \frac{\langle B_T \rangle V_s}{IR^{1/2}} = k_s \frac{\langle B_T \rangle V_s}{P_0^{1/2}}, \quad [5]$$

where the constant in the above expression is independent of coil geometry but is dependent on sample, B_0, temperature, and bandwidth, and P_0 is the power dissipated in the coil when generating B_T.

Until now, we have considered simply an inductor L with series resistance R. No capacitors are present for tuning or matching. The system is fully broadband. In practice, capacitors are required to provide the proper impedance matching at the frequency of interest. R is typically 0.1 to 1 Ω at radiofrequencies and the inductive reactance is typically 20 to 200 jΩ. For efficient matching both to the RF pulse transmitter and to the preamp, and for efficient signal transfer over available cables, the impedance must be transformed to typically 50 Ω resistive (*5, 6*). If the transformation is lossless, the signal-to-noise is unchanged. If losses are involved but the two-port transformation is passive, the losses must be symmetrical. (The admittance matrix of a passive two-port network is positive semidefinite Hermitian (*7*).) Thus, the efficiency of delivering RF power to the coil in generating B_T will be identical to the efficiency of transferring signal power back through that same transformation circuit to a preamp. The required pulse power for a given B_T is increased by the reciprocal of the efficiency while the

signal power is reduced by the same efficiency factor. Hence, the validity of Eq. [5] is unaffected when we replace coil power with input pulse power. Using Eq. [2], we may now write

$$S/N \propto \frac{V_s}{t_{90}P^{1/2}}, \qquad [6]$$

where t_{90} is the mean time required to rotate the magnetization 90° over the sample volume V_s with pulse power P. The above expression allows simple comparisons between different probes, regardless of the impedance transformation network (single, double, or triple tuned, etc.) by a simple measurement of the mean t_{90} over V_s at a determined power level. This expression adequately considers linear probe design considerations such as coil losses, efficiency, filling factor, lead losses, capacitor losses, and Q's for a given sample, etc. It does not always allow accurate comparisons between different probes on different samples because it does not explicitly consider sample losses and it ignores the effects of both RF and B_0 field inhomogeneity. Also, it assumes free spins. Hence, it ceases to allow accurate comparisons between different resonators when radiation damping (*3*) is significant, which may be the case in high-field proton NMR on concentrated samples. Finally, it is not valid when nonlinear switching elements are present, as in certain damping circuits.

LOW-TEMPERATURE CIRCUITS

Before leaving the topic of thermal noise, we should note the obvious square root temperature dependence in Eq. [3] and some often overlooked effects. The above expressions for S/N all assume a noiseless preamp. The most common method of rating the noise performance of a preamp is to write a noise figure in decibels equal to the noise power added by the preamp,

$$\mathrm{NF} = 10 \log \frac{V^2/R_L}{N^2/R_s} - G, \qquad [7]$$

where V is the rms output noise voltage when the preamp input R_s is a pure resistor at 290 K, G is the power gain of the preamp, and R_L is the load resistance. N is obtained from Eq. [3] for R_s at 290 K with the same bandwidth as is used when measuring V. In practice, one normally measures V for two different known temperature noise sources (e.g., 290 and 77 K, or 295 K and a calibrated noise diode equivalent to perhaps 3000 K) so as to eliminate G from Eq. [7] and to require only a knowledge of N_H/N_C. For example, using a 50 Ω source at 77 K for V_c and a 50 Ω source at 290 K for V_H with a constant load impedance on the preamp gives

$$\mathrm{NF} = 10 \log\left(\frac{0.735}{1 - (V_c/V_H)^2}\right). \qquad [8]$$

Figure 1 shows the relationship between NF and an equivalent representation, noise temperature T_N.

The primary object of this digression on preamp NF is to point out the significance of even a slight reduction in preamp NF when the NMR coil circuit is cold. The NF indicates the noise added to a room temperature resistor. Typical broadband NMR

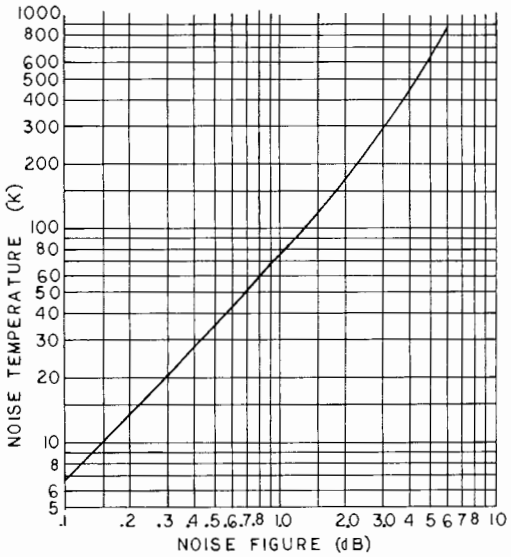

FIG. 1. Relationship between noise temperature and noise figure.

spectrometers have system noise figures (duplexer, preamp, mixer, IF) of about 1.4 to 1.8 dB. Using broadband (5–300 MHz) 50 Ω preamps developed in our lab, the system noise figure can be reduced to 0.8 dB. Reducing the preamp NF from 1.8 dB (noise temperature T_N = 149 K) to 0.8 dB (T_N = 59 K) results in a rather modest 15% increase in the S/N ratio when the NMR coil is at room temperature. However, if the coil and capacitors are at 4 K, the S/N enhancement is about 50%. Note that this enhancement is independent of the large enhancements due to the increased coil Q and increased Boltzman factor in the magnetization. However, if the capacitors are at room temperature while the coil is at 4 K, their losses will generally dominate the total Q and hence the thermal noise. In this case, the Q will be increased by perhaps a factor of two or three but the effective circuit noise temperature is not significantly lowered.

ABSOLUTE EFFICIENCY

It is instructive and useful to ask if it is possible to derive a theoretical limit to S/N that can readily be compared to simple probe-dependent measurements. We could then speak of an absolute efficiency. The derivation is straightforward.

The ideal probe would generate uniform, circularly polarized magnetic fields over the sample volume V_s, with vanishing magnetic fields elsewhere. The Q should be as high as permitted by bandwidth constraints except in the rare case where radiation damping is a problem.

Directly from energy storage considerations (*5, 8*) we derive the minimum power requirement for a uniform, confined field of magnitude B_1 when sample dimensions are small compared to the wavelength:

$$P = \frac{1}{2Q\mu_0} B_I^2 V_s \omega \qquad [9]$$

$$B_I = \left(\frac{2PQ\mu_0}{V_s\omega}\right)^{1/2}. \qquad [10]$$

While such a resonator does not exist in practice, the "birdcage resonator" (*9*) is a reasonable approximation, and the ideal thin toroid and infinite solenoid are off by only a factor of two in power as a result of linear polarization instead of circular polarization of the magnetic field.

We define the absolute efficiency, η_0, as the ratio of the measured B_1^2 to the ideal B_I^2, the maximum that can possibly be obtained for a given Q, P, ω, and V_s:

$$\eta_0 = \left(\frac{B_1}{B_I}\right)^2 = \frac{\langle B_1\rangle^2 \omega V_s}{2PQ\mu_0} \qquad \text{(mks)}. \qquad [11]$$

The above equation is in mks units. It is often convenient to convert to mixed units. With B_1 in G, f in MHz, V_s in cm^3, and P in W,

$$\eta_0 = \frac{0.025\langle B_1\rangle^2 f V_s}{PQ} \qquad \text{(mixed)}. \qquad [12]$$

It is important to keep in mind that B_1 is an average over the sample volume, and Q is the isolated, loaded Q of the circuit and sample system (X_L/R_s, or R_p/X_L), which is twice the system Q when connected to a matched load. The Appendix shows that the isolated Q may be measured with a return loss or reflectance bridge as follows,

$$Q = \frac{f_0}{\Delta f_{7\,\mathrm{dB}}} \qquad [13]$$

where $\Delta f_{7\,\mathrm{dB}}$ is the bandwidth for which the reflected power of the matched circuit is 7 dB below the incident power. This technique is equivalent to the frequently quoted, but difficult to implement, −3 dB extreme-under-coupled technique (*10*). This Q includes losses arising from all coils, capacitors, resistors, eddy currents in nearby conductors, and dielectric losses.

Using the experimentally determined B_1 for B_T in Eq. [4], along with Eq. [11] and the Lamor equation, gives

$$S/N \propto (\eta_0 Q V_s)^{1/2} \omega^{3/2}. \qquad [14]$$

The (perhaps unexpected) square root dependence on sample volume is merely a manifestation of the fact that our absolute efficiency includes all circuit parameters (except Q), one of which is filling factor. One useful aspect of the concept of absolute efficiency is that it allows a simple, Q-independent comparison of various coils, resonators, and transformation circuits. The Q is explicitly retained in the expression because of its importance in bandwidth and ringdown considerations.

It is interesting to look at the absolute efficiencies of some typical, high-efficiency probes as shown in Table 1. The absolute efficiencies are surprisingly low. This should not give false hopes for dramatic possibilities of improvements. Quite to the contrary,

TABLE 1

Experimental Comparison of Several Probes

Probe	Coil type	Nucleus	f (MHz)	V_s (cm^3)	P (W)	Q	B (G)	η_0
5 mm CPMAS	Solenoid	^{13}C	125	0.13	200	250	58	0.027
7 mm CPMAS	Solenoid	^{1}H	300	0.33	90	320	15	0.019
7 mm CPMAS	Solenoid	^{13}C	75	0.33	250	260	58	0.032
10 mm high resolution	Saddle	^{13}C	75	1.15	100	230	12	0.014
254 mm imaging	Solenoid	^{1}H	6.9	13,000	200	85	0.63	0.052

the authors feel that only marginal improvements are possible. However, it may give some insight into one of the reasons MRI has been able to make progress far beyond anyone's early expectations. In large sample resonators, the absolute efficiency can be an order of magnitude larger than in typical small coils.

The main contributions to low absolute efficiency in conventional coils are (1) the usually unavoidable linear polarization instead of circular polarization (a factor of 0.5); (2) the low geometric filling factors (typically 0.3) that are encountered in small coils, especially in MAS; and (3) the large external or nontransverse RF fields that normally are produced (typically a factor of 0.25). Lead losses, when double tuning, multinuclear capability, and high power are required, can also account for an additional factor of 0.5.

Figure 2 shows a typical high-power double-tuned 400/100 MHz multinuclear circuit with typical major losses. The sample coil is four turns of 2.2 × 0.2 mm flat copper on an 8 mm diameter × 12 mm cylindrical form. Total low-frequency (LF) series inductance at 100 MHz has been reduced to the minimum practical amount that permits (1) efficient LF multinuclear tuning, (2) variable temperature, (3) high power, and (4) MAS. Yet, the actual coil inductance is little more than half of the total series inductance. If further reductions in lead inductance could be obtained (within the

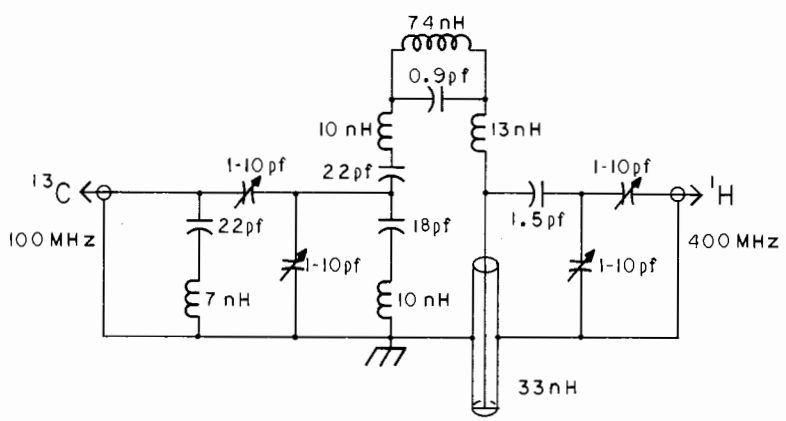

FIG. 2. Double-tuned circuit with typical parasitic inductances.

above experimental constraints) the major benefit would be an increase in the maximum RF field attainable before the onset of high-voltage breakdown. The effect on sensitivity would be negligible, since wide foil leads are used which contribute a negligible amount to the total series resistance. Although the coil losses are dominant, the fixed capacitor losses are nearly as large even when the highest quality, high-voltage capacitors are used.

SPURIOUS NOISE

The term "spurious" has traditionally been used to refer to any unwanted signals in RF that cannot be attributed to well-characterized noise sources such as thermal, shot, $1/f$, fixed unwanted signals, or catastrophic breakdown. It especially is used to refer to products appearing as a result of mixer or preamp overload. We discuss here two nonlinear effects we have observed in high-power double-tuned NMR probes—partial capacitor failure and contact junction noise. Being nonlinear, these problems are manifest only when high power is being applied at one frequency while observing a second.

HIGH-VOLTAGE CAPACITOR NOISE AND BREAKDOWN

If a 5 pF, 5 kV capacitor is placed in series with a 20 pF, 500 V capacitor, the effective voltage rating of the combination is 2.5 kV, not 5.5 kV, since the voltage across each capacitor is inversely proportional to its capacitance,

$$V_i = V_T \frac{C_T}{C_i}, \qquad [15]$$

where V_T is the total voltage and C_T is the total series capacitance. Thus, the voltage across the 5 pF capacitor will be 2 kV when the 20 pF capacitor begins to breakdown at 500 V.

A totally analogous situation occurs in a single capacitor with two dissimilar dielectrics. Consider the dielectric-air, parallel plate capacitor as shown in Fig. 3, with dielectric thickness d, air gap g, and dielectric constant k.

This is essentially two capacitors in series, with total capacitance C_T given by

$$C_T = \frac{C_d C_g}{C_d + C_g} = A\epsilon_0\left(\frac{k}{d + gk}\right). \qquad [16]$$

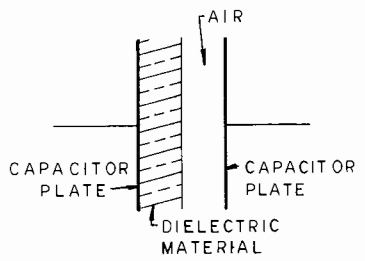

FIG. 3. A parallel plate capacitor with an air gap.

The voltage gradient in the air gap is readily shown to be

$$V/g = \frac{V_T k}{d}. \quad [17]$$

Thus the voltage gradient in the air gap, compared to a similar capacitor with only air as the dielectric, is increased by a factor equal to the dielectric constant of the second material. However, the RF voltage gradient that air (and other dielectrics) will withstand is generally inversely proportional to the square root of the thickness (*11*), for dimensions that are very large compared to interatomic distances and small compared to a wavelength. Hence, the breakdown voltage V_{BD} of the dielectric-air capacitor due to breakdown in the air gap, relative to the breakdown voltage V_{BA} of a similar air-only capacitor, is

$$V_{BD} = V_{BA}\left(\frac{d}{g}\right)^{1/2} \Big/ k. \quad [18]$$

For a coaxial capacitor with a substantial difference between the inner and outer diameter, the situation becomes much more critical at the inner diameter since the voltage gradient is inversely proportional to the radius. For a coaxial resonator with a PTFE insulator ($k = 2.1$) and a ratio of outer diameter to inner diameter of 3, the air gap between the center conductor and the insulator must be less than 1/40 of the Teflon thickness in order for the breakdown voltage with the insulator present to exceed the voltage breakdown for an air-only parallel plate capacitor of equivalent separation distance.

Breakdown in a small air gap does not result in a large spark and will usually not be detectable in the reflected power since the energy is quite low. In fact, the probe may continue to function quite well in single-tuned service until substantial damage has occurred. The spark energy U is

$$U = \tfrac{1}{2} CV^2. \quad [19]$$

For the parallel plate situation of Fig. 3, the ratio of energy in the air gap to energy in the dielectric is

$$\frac{U_A}{U_T} = \frac{gk}{d}. \quad [20]$$

The NMR signal is typically 10^9 to 10^{15} times smaller than the decoupling power. Thus, even the smallest breakdown may mask the NMR signal. When breakdown occurs, the small, local air capacitor discharges rapidly. The spectral density of the noise is essentially uniform at frequencies well below the reciprocal of the discharge pulse width. A 10 pF air capacitor, charged to 100 V and abruptly discharged at 100 MHz can generate a noise density well in excess of the thermal noise across a bandwidth of tens of gigahertz without any visible sign of arcing, either visually or in reflected power. Excess noise from 10 to 40 dB beyond the thermal level (thermal noise = −168 dBm/Hz) has been attributed to this mechanism. The only acceptable solution is to assure that all air gaps are small enough so that no breakdown occurs.

We have observed the above problem most frequently in λ/4 resonant lines, coils wound on dielectric forms, and in quartz variable capacitors. It also sometimes occurs

in the terminations of faulty chip capacitors and in airspaces between high-voltage points and other dielectric insulators. We have seen this phenomenon occur just prior to catastrophic breakdown of the quartz dielectric in common 1–10 pf "10 kV" quartz capacitors from several manufacturers (JMC and Voltronics) at about 2.1 to 2.4 kV at 300 MHz at about 40% relative humidity, with the lower cost JMC devices consistently showing both slightly higher Q and slightly higher voltage breakdown. The amount of ozone generated by these low-energy discharges is usually not discernible, even when the amount of noise generated is 30 dB above thermal, while visible corona and major sparking will usually produce a readily detectable level of ozone and a substantial change in reflected power.

TRIBOELECTRIC NOISE

Triboelectric noise generated by the high-velocity air over the surfaces of the spinner system in MAS can be a difficult problem at very high spinning speeds. This noise is minimized by using materials for the spinner system that have triboelectric potentials similar to that of air (*12*)—e.g., ceramics and polyimides rather than fluorinated plastics. Triboelectric noise may be clearly identified by observing its decrease when using spinning air with high humidity. (This is likely to seriously exacerbate high-voltage breakdown problems, as reduced breakdown voltages are in fact often the result of moisture in the compressed gas supply.) In extreme cases, a visible glow may be seen around the spinner turbine with no RF power applied.

Highly nonpolar dielectrics such as PTFE and PE readily accumulate surface static charges at high potentials as a result of this triboelectric effect when air is moving over their surfaces. In addition, asymmetrical leakage currents in a series capacitor circuit can result in large initial polarization of the dc isolated nodes in the circuit. Thus, it is common to observe short, random bursts of noise during the first several seconds of high-power operation until surface charges are removed and isolated capacitors are depolarized. These noise spikes may be 6 to 40 dB above thermal noise, but they are usually at a relatively low random repetition rate (perhaps several hundred hertz) and under a microsecond in duration. Hence, the integrated effect on S/N may be quite small after proper filtering.

It is common to use a dual level proton power scheme to allow proton decoupling at a higher power level than the cross-polarization period will permit due to observe power limitations. For the highest decoupling powers, it may be necessary to use a trilevel scheme in which a brief decouple pulse at higher decoupling power is applied during the observe ringdown period, just prior to acquisition, to ensure that surface charges are removed and capacitors are fully depolarized, before beginning signal acquisition at a slightly lower proton power level.

CONTACT JUNCTION NOISE

When current flows across a nonlinear junction, the discrete nature of the charge carriers gives rise to a statistical fluctuation, known as shot noise or Schottky noise. Schottky gives the value of this mean square fluctuation (*13*) as

$$\langle I_N^2 \rangle = 2qI\Delta f, \qquad [21]$$

where q is the electron charge, I is the current in question, and Δf is the noise bandwidth. This noise current will produce a noise power $I_N^2 R$ in a resistor. This noise extends from dc to hundreds of gigahertz with uniform spectral density.

A typical double-tuned NMR coil will have a series resistance of about 0.5 Ω at the observe frequency with about 10 A of decoupler current flowing through it, and perhaps 20 A of decoupler current will be present in a 0.2 Ω $\lambda/4$ resonator. The Schottky noise power that could be generated in a nonlinear coil circuit junction is then at least −145 dBm/Hz, 23 dB above thermal noise.

Higher resistance nonlinear junctions are not only possible but also probable if extreme care is not exercised. Aluminum is often used for structural elements because of its light weight and nonmagnetism even though its tendency to oxidize quickly makes adequate electrical contact difficult. In multinuclear probes, the RF resonant current is required to make long paths to accommodate the high-power variable capacitors. Substantial RF current is induced in virtually every conductor present in the probe structure. If the probe contains structural elements of length close to $\lambda/4$ that are open at one end (or structural elements that are close to $\lambda/2$ that are open or grounded at both ends), the ground loop problems are greatly increased, and additional resonances will appear, causing tuning difficulties. If such unwanted resonances appear, it is usually possible to damp them by a judiciously placed resistor, thereby greatly simplifying tuning and reducing ground loops.

Ground loops of dimensions on the order of centimeters can have tens of nanohenrys inductance. The relative energy in any given loop (at the proton frequency, for example) may be shown to be approximately twice the relative effect on the resonant frequency when that loop is broken. For example, if the resonant frequency shifts by 1% when two ground fingers contact the shield can, then the energy in the ground loop between the two ground fingers is about 2% of the total resonant energy. The power dissipated in that ground loop may be substantially greater or less than 2%, depending on the Q of that loop relative to the total Q. If the loop has 2% of the total resonant energy at half the inductance of the $\lambda/4$ resonator, then the current flowing in that loop is about 1/5 of the primary current. Four amperes of current through 10 nH inductance at 400 MHz requires an emf of over 100 V, well beyond the band gap of aluminum oxide, copper oxide, silver sulfide, or any other insulating thin film that may be present, and thus will generate an unacceptable amount of shot noise if contact resistance is beyond several milliohms. The fraction of noise power generated here at the observe frequency which ends up at the observe port is not the same as the above relative power dissipation since the frequencies are different, but it is typically of the order of 1%. Reducing contact noise in high-power double-tuned probes requires care in positioning of the contacts so that they are at equipotential points at the decoupling frequency. This is particularly true of the contacts used in capacitor switching in multinuclear circuits, since noise generated in these contacts will be coupled very efficiently to the observe port.

Since aluminum welding is difficult, and aluminum soldering requires toxic alloys of cadmium, zinc, and silver with rather caustic fluxes, we have tried (much to our grief) various silver paints and silver-filled epoxies to ensure adequate electrical ground connections at aluminum–aluminum and aluminum–copper junctions. Spray-on silver paints with polymeric binders have resistivities of about 0.01 Ωcm making them useless

for RF grounding or RF shielding. Silver-filled epoxies are widely used with success in various surface mount printed circuit applications; but we have not found any with resistivities much below 0.01 Ωcm, and 0.03 Ωcm is common. In addition, they have very high positive temperature coefficients and are microphonic and somewhat nonlinear. Hence, they too have disastrous consequences if used in critical grounding applications in RF circuits without supplementing with high-conductivity silver paint or welding.

High silver content (65–70%) paints with nearly 100% volatile vehicle (toluene) can be used successfully to establish adequate electrical connections between aluminum and other metals if the surfaces are well cleaned prior to application of the paint and the joints are mechanically very rigid. Resistivities after room temperature drying are below 2×10^{-4} Ωcm. The only drawback is that if the junction is subjected even to very slight mechanical strain, the paint may crack and flake. We have seen long-term satisfactory service from many probes relying on high silver content paint to make electrical contact between an aluminum structure and a copper RF line that has been rigidly secured with epoxy, but we have recently begun using TIG (tungsten electrode with inert gas coverage) welding, press fit joining, and aluminum soldering alloys for improved reliability.

The importance of having 100% high integrity electrical contacts throughout the entire probe cannot be overemphasized. In places where it is difficult to ensure reliable contacts—such as capacitor adjustment or changing mechanisms—it is best to use ceramics or plastics or to place insulation between metal surfaces that could make intermittent contact.

MISCELLANEOUS NOISE CONSIDERATIONS

The above reliable contact problem extends beyond the probe to the high-power decoupler amplifier, RF cables, duplexers, etc. Highest quality double-shielded cables must be used for all high-power transmission lines to minimize radiation and the likelihood that it will result in spurious mixing products or shot noise within the observe spectrum. Likewise, highest quality double-shielded cable must be used on all small signal transmission lines to minimize noise pickup from general atmospheric radio noise and from local sources that are generated by the decoupler amplifier leakage. Low-loss filters (that do not suffer from nonlinearities at the incident decoupler power level) are required to reject noise at the observe frequency from the decoupler amplifier and to reject the high-level decoupler frequency at the observe preamp, but they are clearly of no value in rejecting spurious noise at the preamp within the observe spectrum. High-power testing is essential, since the voltages generated within a filter are often much higher than expected—especially in very sharp cutoff and tuned filters near the edge of the passband. Careful construction techniques are required in the decoupler amplifier to ensure that it does not leak significant power at the decouple frequency that could result in spurious noise and that it generates and broadcasts extremely low levels of noise throughout the full spectrum.

Atmospheric noise seen by an antenna is usually at least 10 dB above thermal under best conditions (*14*), and may be 80 dB above thermal under adverse conditions. This, and noise generated by local instrumentation, must be prevented from entering the

probe on the heater and thermocouple lines and on the spin rate monitoring system used in MAS. Capacitive bypassing and shielding are required on the heater and thermocouple. In addition, low-frequency magnetic fields generated by the probe heater, magnet shims, and gradient coils in the sample region must be small compared to the minimum spectral linewidths, since this low-frequency noise cannot be shielded.

Triboelectric-based spin rate monitoring systems are easily RF isolated with a 47 kΩ resistor and a 100 pF capacitor. Fiberoptics spin rate monitoring systems should present no problem unless electric field gradients around the metal ferrule on the end of the fiber bundle result in low-energy discharges.

PREAMP CONSIDERATIONS

We return now to the preamp to mention several additional specifications of importance to high-power NMR applications. In addition to the obvious requirement of adequate pulse protection without degrading the noise figure, it is often important to minimize recovery time from saturation without significant sacrifice of NF or low-frequency response. A 5 μs recovery time can be obtained in a properly designed 1 dB NF, 5–300 MHz preamp, and this is usually sufficient. Recovery times of 0.5 μs may be required for proton multipulse experiments. This requires an order of magnitude increase in the low-frequency limit or a considerable sacrifice in NF. Probe ringdown time is often more of a limitation than preamp recovery time. Since preamp input VSWR is typically greater than 2 for minimum noise, it is possible to decrease probe ringdown time by a large factor by adjusting the cable length and impedance matching, although S/N will probably suffer slightly. In most cases dynamic range is not a significant problem and 30 to 35 dB of preamp gain is found to be optimum for simplifying design of the filters, mixer, attenuators, and IF amplifier following the preamp. With more attention to mixer conversion loss, IF noise figure, and filter losses, the preamp gain can be reduced to 20 dB for increased dynamic range without loss of sensitivity. Increasing the dynamic range and improving linearity (increasing third-order intermodulation intercept) can be beneficial in reducing spurious noise from high-level decoupler signals.

APPENDIX: Q MEASUREMENT

The quality factor Q of a series R_sLC circuit, as in Fig. 4a, is normally defined as

$$Q = \omega_0 L/R_s = 1/R_s\omega_0 C. \quad [1]$$

At resonance, R_s may be measured by a direct resistance measurement, if suitable equipment is available. However, R_s is usually too small for this technique.

The impedance at frequency $\omega_0(1 \pm \epsilon)$ for $Q \gg 1$ is

$$Z = R_s + j\omega_0 L(1 \pm \epsilon) - \frac{1}{j\omega_0 C(1 \pm \epsilon)} \quad [2]$$

$$\simeq R_s + \left(j\omega_0 L - \frac{1}{j\omega_0 C}\right) + 2\epsilon j\omega_0 L \quad [3]$$

$$= R_s \pm 2\epsilon j\omega_0 L = R_s \pm 2\epsilon jQR_s. \quad [4]$$

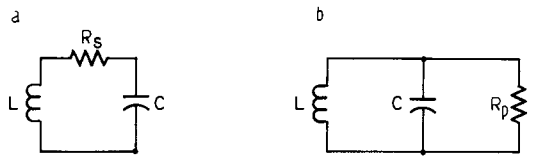

FIG. 4. Series and parallel representations of circuit losses.

For $\epsilon = 1/2Q$, the real and imaginary parts are equal. Thus, for $Q \gg 1$, we have an alternate definition of Q,

$$Q = \frac{\omega_0}{\omega_2 - \omega_1}, \qquad [5]$$

where ω_1 and ω_2 are the frequencies at which the phase angle is $\pm 45°$. It can also be shown that these are the half power frequencies, and that the R_p of Fig. 4b is equal to $Q\omega L$. Again, the Q may be determined by either of the above relationships, if suitable equipment is available. However, it is usually easier to measure a reflection coefficient, Γ, than an impedance phase angle, or a half power point, or a parallel impedance, without perturbing the system:

$$\Gamma = \frac{V_r}{V_i} = \frac{Z_L - Z_0}{Z_L + Z_0}. \qquad [6]$$

V_r and V_i are the reflected and incident voltages and Z_0 and Z_L are the line and load impedances.

The return loss, or relative reflected power, is given by the square of the reflection coefficient. For a phase angle of $\pm 45°$, we have, for the series RLC circuit,

$$\frac{P_r}{P_i} = |\Gamma|^2 = \left|\frac{(Z_0 \pm jZ_0) - Z_0}{(Z_0 \pm jZ_0) + Z_0}\right|^2 = \left|\frac{\pm j}{2 \pm j}\right|^2 = \frac{1}{5}. \qquad [7]$$

Thus, the reflected power from a tuned circuit that is matched to the line impedance at resonance will be 1/5 (or -7 dB) of the incident power at frequencies $\omega_0 + \omega/2Q$ and $\omega_0 - \omega/2Q$. The reflection coefficient measurement may be calibrated using a resistive load of either $0.382Z_0$ (19.1 Ω for a 50 Ω line) or $2.618Z_0$ (131 Ω), since the return loss of these two resistances is also 7 dB:

$$\left|\frac{0.382 + 1}{0.382 - 1}\right|^2 = \left|\frac{2.618 + 1}{2.618 - 1}\right|^2 = \frac{1}{5}. \qquad [8]$$

When calibrating and using the reflectance measurement system, it is important to remember that cable lengths transform nonmatched impedances, and the only simple transformation is for a cable length of $n\lambda/2$, which gives a transformation of unity. The cable lengths on the 19.1 or 131 Ω calibration loads can usually be made close enough to zero, and the cable length from the matching capacitor in the tuned circuit inside the probe to the reflectance bridge or 0-0-0-180 hybrid junction can usually be made equal to $\lambda/2$.

Finally, although Eq. [7] is strictly valid only for the simple series circuit (where the real component is independent of frequency), it can be shown to be approximately true for any high Q circuit, and the technique is widely applicable to all high Q circuits.

ACKNOWLEDGMENTS

The authors gratefully acknowledge spectrometer support provided by John Kilpatrick of Varian and Paul Murphy, while with IBM Instruments. Partial support for this research by NIH Contract N44-CM-77804 is also gratefully acknowledged.

REFERENCES

1. D. I. HOULT AND R. E. RICHARDS, *J. Magn. Reson.* **24,** 71 (1976).
2. F. J. TISCHER, "Basic Theory of Space Communications," Van Nostrand, Princeton, New Jersey, 1965.
3. F. D. DOTY, "Resonator Sensitivity Optimization in Magnetic Resonance and the Development of an MAS Probe for the NMR Study of Rare Spin Nuclei," Doctoral Dissertation, University of South Carolina, 1983.
4. F. N. H. ROBINSON, "Noise and Fluctuations," Oxford Univ. Press (Clarendon), London/New York, 1974.
5. F. D. DOTY, R. R. INNERS, AND P. D. ELLIS, *J. Magn. Reson.* **43,** 399 (1981).
6. Y. J. YIANG, R. J. PUGMIRE, AND D. M. GRANT, *J. Magn. Reson.* **71,** 485 (1987).
7. R. S. CARSON, "High Frequency Amplifier Design," Wiley, New York, 1982.
8. C. P. POOLE, "Electron Spin Resonance," Interscience, New York, 1967.
9. C. HAYES, W. EDELSTEIN, J. SCHNECK, O. M. MUELLER, AND M. EASH, *J. Magn. Reson.* **65,** 622 (1985).
10. D. I. HOULT, *Prog. NMR Spectrosc.* **12,** 41 (1978).
11. J. J. O'DWYER, "The Theory of Electrical Conduction and Breakdown in Solid Dielectrics," Oxford Univ. Press, London, 1973.
12. "Motorola Power Mosfet Transistor Data," Motorola Semiconductor Products, Inc., Phoenix, Arizona, 1984.
13. J. WATSON, "Analog and Switching Circuit Design," Adam Hilger Ltd., Bristol, 1984.
14. M. J. Wilson (Ed.), "The ARRL Handbook," ARRL, Newington, Connecticut, 1987.